

# Controlled motility in the cyanobacterium *Trichodesmium* regulates aggregate architecture

Ulrike Pfreundt<sup>1†</sup>, Jonasz Stomka<sup>1†</sup>, Giulia Schneider<sup>1</sup>, Anupam Sengupta<sup>2</sup>, Francesco Carrara<sup>1</sup>, Vicente Fernandez<sup>1</sup>, Martin Ackermann<sup>3,4</sup>, Roman Stocker<sup>1\*</sup>

The ocean's nitrogen is largely fixed by cyanobacteria, including *Trichodesmium*, which forms aggregates comprising hundreds of filaments arranged in organized architectures. Aggregates often form upon exposure to stress and have ecological and biophysical characteristics that differ from those of single filaments. Here, we report that *Trichodesmium* aggregates can rapidly modulate their shape, responding within minutes to changes in environmental conditions. Combining video microscopy and mathematical modeling, we discovered that this reorganization is mediated by “smart reversals” wherein gliding filaments reverse when their overlap with other filaments diminishes. By regulating smart reversals, filaments control aggregate architecture without central coordination. We propose that the modulation of gliding motility at the single-filament level is a determinant of *Trichodesmium*'s aggregation behavior and ultimately of its biogeochemical role in the ocean.

The input of new nitrogen into the ocean and thus global primary productivity is driven in large part by nitrogen fixation by only a few types of cyanobacteria (1), one of them being the genus *Trichodesmium* (2, 3). Oceanographers have been puzzled by *Trichodesmium*'s dual occurrence as either single multicellular filaments or aggregates comprising hundreds of filaments (4–6). Both often occur in the same water and are found in all tropical and subtropical oceanic ecosystems (6, 7) and across different *Trichodesmium* species (8). In laboratory conditions, aggregation of *Trichodesmium* filaments typically occurs in the postexponential growth phase (9–11). It can also be induced by depleting iron or phosphate (12), reducing salinity (11), or changing growth medium or irradiance (13). This suggests that aggregation is a general stress response. Compared with filaments, aggregates perform different ecological and metabolic functions (14–21), partially due to the microbiomes they host (22, 23). Aggregates create different microenvironments (24, 25) that may be transiently suboxic and thus reduce nitrogen and carbon fixation compared with single filaments (26). However, through behaviors inaccessible to single filaments, aggregates have better access to other limiting resources. They can capture iron-loaded dust (14, 18, 27), which may help aggregates engage in iron-intense nitrogen and carbon fixation simultaneously, a hallmark of

*Trichodesmium* ecology (28). Aggregates may be able to scavenge phosphate from the depths by rapid vertical migration (15, 29), and *Trichodesmium* aggregates at depths below 170 m have been observed to fix nitrogen at similar rates as aggregates in the surface ocean (30). Vertical migration is likely also involved in the formation of surface blooms (31) spanning tens of thousands of square kilometers (32–34). However, despite the notable ecology of *Trichodesmium* aggregates little is known about the mechanisms by which filaments give rise to aggregates, how aggregate architecture is controlled, and on what timescale this control occurs. We report that *Trichodesmium* aggregates are active filament assemblies capable of rapid structural changes in response to changes in environmental conditions and we show that this active reshaping of aggregates is realized by changes in the motility of individual filaments.

## Changes in light exposure induce rapid reshaping of aggregates

We analyzed the effect of changing light conditions on aggregates of *Trichodesmium erythraeum* IMS101, a strain frequently associated with open-ocean surface blooms (35). Changes in light intensity are an ecologically relevant cue, occurring in the surface ocean due to cloud movement and can induce cellular stress by generating reactive oxygen species (ROS) (36). We exposed naturally aggregating *T. erythraeum* cultures in the late stationary growth phase to sudden changes in light intensity (light switches) (Fig. 1) and quantified the size and density of individual aggregates over ~30 hours through time-lapse imaging.

Aggregates responded rapidly to light switches (movie S1 and Fig. 1). After a Light OFF switch, aggregates expanded (Fig. 1, A and B)—the same set of filaments in the aggregate rearranged into a looser and larger aggregate—

causing the average density to decrease by 10% (mean  $\pm$  SEM,  $n = 18$ ) over 24 min (Fig. 1, C and E, and movie S1). Conversely, after a Light ON switch aggregates tightened causing the average density to increase by  $26 \pm 17\%$  (mean  $\pm$  SEM,  $n = 30$ ) over 65 min (Fig. 1, D and F, and movie S2). The pure circadian onset of the night phase (blue horizontal bar, Fig. 1D) but with the light kept on did not lead to aggregate loosening. Only when the light was actually turned off did the aggregates loosen (at 10 hours, Fig. 1D). Although this does not exclude circadian control of aggregation behavior, it shows that the observed responses were inducible by light changes irrespective of the time of day. Responses were rapid, starting to be visible within 0 to 8 min of a switch (Fig. 1, E and F) and were transient and reversible, i.e., aggregates returned to approximately their previous configuration after cessation of the light perturbation. A UV-killed control culture did not form aggregates (movie S3). The structural configuration of an aggregate can thus change over timescales of minutes, suggesting that active movement is implicated in aggregate loosening and tightening. These experiments also revealed that puff-like aggregates often formed sequentially: individual filaments first aggregated into tight bundles (tufts), which in turn encountered one another and rearranged into puffs (movie S4). This process was also observed to occur in reverse, whereby a puff disintegrated into several tufts (movie S4).

## Filament–filament interactions reveal a motility mechanism to modulate aggregate shape

*Trichodesmium* filaments can glide on surfaces (12, 18, 37) (movies S5 and S6) through an as-yet unknown locomotion mechanism. We discovered that filaments can also glide on each other without the presence of another surface, in experiments in which we suspended a filament in liquid using a micropipette and brought a second filament into contact with it by fluid flow (movie S7). Upon meeting, the two filaments started gliding against each other without any contact to a solid surface (except the pipette tip). We next characterize the motility of individual filaments and filament pairs and show that filament–filament gliding is a component—although by itself not sufficient—of aggregate reshaping.

Individual *Trichodesmium* filaments move in a series of nearly straight, fast “runs” interrupted by periods of slower motion, which we term reorientations (Fig. 2A). Analyzing the tracks of hundreds of individual filaments (Materials and Methods, Supplementary Text Section I) on the glass surface of a microfluidic chamber (movie S8), we found that filaments glide at  $34.1 \pm 31.9 \mu\text{m min}^{-1}$  (mean  $\pm$  SD,  $n = 776$ ), primarily along their long axis (fig. S1). Run times exhibit a broad distribution

<sup>1</sup>Institute of Environmental Engineering, Department of Civil, Environmental and Geomatic Engineering, ETH Zurich, Zurich, Switzerland. <sup>2</sup>Physics of Living Matter, Department of Physics and Materials Science, University of Luxembourg, Luxembourg City, Grand Duchy of Luxembourg. <sup>3</sup>Department of Environmental Systems Sciences, Microbial Systems Ecology Group, Institute of Biogeochemistry and Pollutant Dynamics, ETH Zurich, Zurich, Switzerland. <sup>4</sup>Department of Environmental Microbiology, Eawag: Swiss Federal Institute of Aquatic Sciences, Dübendorf, Switzerland.

\*Corresponding author. Email: romanstocker@ethz.ch

†These authors contributed equally to this work.



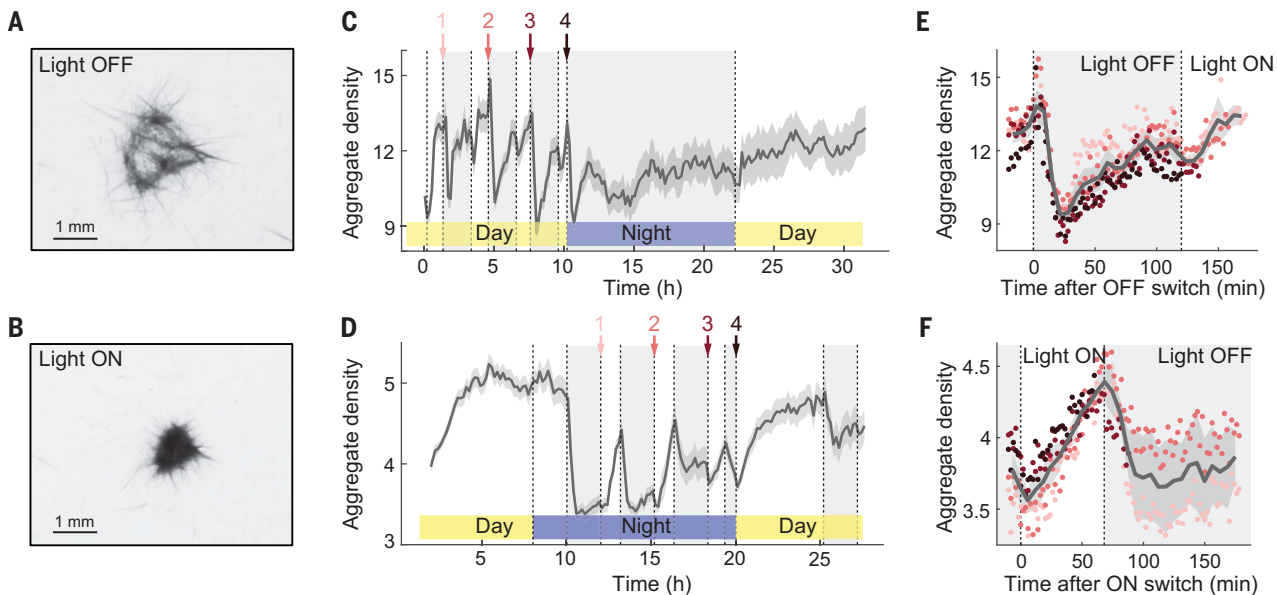


**Fig. 1. *Trichodesmium* aggregate density changes rapidly upon switches in light intensity.** (A and B) A puff aggregate in its loose form 15 min after a Light OFF switch (A) and in its dense form in  $80 \mu\text{mol quanta m}^{-2} \text{s}^{-1}$  light (B). (C and D) Time series of mean aggregate density (i.e., the density of filaments within aggregates, quantified as the mean pixel intensity of individual aggregates) in light-switching experiments, with four Light OFF switches (numbered arrows) during the day (C) and four Light ON switches (numbered arrows) during the night (D). Switch 4 corresponds to the normal onset of the next night/day, respectively. Light conditions were  $80 \mu\text{mol quanta m}^{-2} \text{s}^{-1}$  in all cases. (E and F) Overlays of the four Light OFF switches (E) from (C) and the four Light ON switches (F) from (D), color-coded from pink (switch 1) to dark red (switch 4), with each data point representing the mean aggregate

density of all aggregates in the imaging frame (16 to 19 aggregates in (E) and 26 to 31 aggregates in (F)). In (C to F), aggregate density (arbitrary units) was computed as the mean pixel intensity per aggregate. Note the different scales in (C and D) and (E and F) resulting from the fact that aggregate density is measured as pixel intensity and thus not directly comparable among experiments (Materials and Methods). The gray curves show a 10-min moving average and the gray shading the 95% confidence interval of the mean. We note that the relation between aggregate density and mean pixel intensity may be nonlinear (because intensity saturates at high aggregate density), however it is monotonic (i.e., higher filament density implies higher mean pixel intensity) and thus pixel intensity represents a useful and convenient metric for aggregate density.

(Fig. 2B) with a mean of  $5.4 \pm 8.2$  min (mean  $\pm$  SD,  $n = 2416$ ). After a reorientation, filaments continue moving in the same direction or reverse, with similar probability ( $57 \pm 1\%$  versus  $43 \pm 1\%$ , respectively; mean  $\pm$  SEM,  $n = 1518$ , Fig. 2C). During a reversal, the leading end becomes the trailing end (movie S9), as also observed previously (12). Gliding motility allows for fast filament movement but filaments lacking the ability to reverse would quickly glide off a nascent aggregate. We thus inferred that reversals are key to aggregation. However, randomly occurring reversals would still cause an aggregate to disintegrate by filaments gliding off it. Consequently, we hypothesized that reversals are triggered by filament–filament contact, thereby allowing an aggregate to reshape without disintegrating.

In aggregating cultures, filaments within pairs had shorter run lengths and thus reversed more frequently than individual filaments. We induced aggregation in mid to late exponential *T. erythraeum* cultures by addition of menadione (Fig. 2D and movie S10), which causes cellular stress through ROS (38). Menadione-induced aggregation is easier to control and thus easier to replicate than relying on post-exponential cultures, in which the exact trigger

for aggregation is unknown. We analyzed individual filaments ( $n = 643$ ) and pairs of filaments that, upon encounter, aligned and glided on each other ( $n = 59$ ). For both categories, we computed filament reversal frequency as well as different gliding motility statistics that might explain changes in the reversal frequency, including run time, run length, reversal probability, and overall activity (i.e., the fraction of time spent in run mode) (table S1). We found that filaments in pairs moved a smaller fraction of their length during a run, 35% less than single filaments ( $0.41 \pm 0.85$  versus  $0.63 \pm 1.52$ , respectively; mean  $\pm$  SD;  $n_{\text{runs,pairs}} = 377$ ,  $n_{\text{runs,single}} = 1964$ ;  $P < 0.001$ , two-sample one-sided Kolmogorov–Smirnov test) (Fig. 2E). Additionally, filaments in pairs spent more time in run mode (table S1), which induced more reorientation events. This higher activity together with shorter run lengths resulted in a reversal frequency that was nearly twice as high in pairs than that in single filaments ( $0.034 \pm 0.040 \text{ min}^{-1}$  versus  $0.019 \pm 0.031 \text{ min}^{-1}$ , respectively; weighted mean  $\pm$  weighted SD;  $n_{\text{pairs}} = 118$ ,  $n_{\text{single}} = 643$ ; weight = track length; Supplementary Text Section II). The fact that a filament in contact with another filament has a markedly higher reversal fre-

quency than single filaments from the same culture suggests that filaments can respond to each other.

To understand how a filament responds to contact with another filament, we measured “lack-of-overlap” of filament pairs. We define lack-of-overlap as the fraction of the shorter filament’s length that does not overlap with the longer filament (Fig. 2F). By tracking both filaments in a pair ( $n = 59$  pairs, as in Fig. 2E), we measured their lack-of-overlap as a function of time (Fig. 2G) to quantify the distribution of lack-of-overlap values. If filaments merely increased their reversal frequency upon contact, the lack-of-overlap would be uniformly distributed (Fig. 2H, Supplementary Text Section III). By contrast, we found that the lack-of-overlap was strongly skewed toward small values ( $P < 10^{-6}$ , one-sample two-sided Kolmogorov–Smirnov test,  $n = 53$ , Fig. 2H). For example, instances of short filaments projecting by less than 50% of their length ( $|\text{lack-of-overlap}| < 0.5$ ) occurred nearly six times more often than filaments projecting by more than 50% ( $|\text{lack-of-overlap}| > 0.5$ ) (Fig. 2H). Thus, the observed increase in reversal frequency upon encounter (Fig. 2E) is not by itself sufficient to describe the behavior

of filaments in pairs. Rather, the prevalence of small lack-of-overlap values suggests that reversals of filaments in pairs are not random but are informed by a sensory cue linked to filament overlap. Thus, reversals are “smart” rather than random. We propose that this behavior is a form of thigmotaxis (39, 40), the change in motility of organisms in response to contact stimuli. In the following, we refer to changes in smart reversals as thigmotaxis, as they are linked to contact between filaments, yet we highlight that the underlying molecular mechanism remains unknown. Such smart reversals are a simple yet effective mechanism for filaments to remain together and rearrange upon encounter. We highlight that filament pairs in the exponentially growing control can also perform smart reversals, however, such pairs disintegrate 2.5 times faster than in the menadione treatment, because filaments in the control perform weaker smart reversals than those treated by menadione, and furthermore because they are faster and shorter (Supplementary Text Section IV; figs. S2 and S3). This faster disintegration rate prevents the formation of stable aggregates in the control.

### Mathematical model of smart reversals

To understand the effects on aggregation of different components of the reversal behavior of filaments, we developed an individual-based model of *Trichodesmium* that represents filaments as motile thigmotactic rods capable of sensing overlap with each other and of reversing when they detect that the overlap is decreasing (Fig. 3). Filaments are represented as highly elongated rods ( $160 \mu\text{m} \times 8 \mu\text{m}$ ), consisting of 20 cells that can glide (speed =  $32 \mu\text{m min}^{-1}$ ) on surfaces and on other filaments, and adhere to each other upon contact, weakly enough to allow relative gliding (fig. S4, Supplementary Text Section V). All filaments reverse randomly (rate =  $32 \mu\text{m min}^{-1} / 160 \mu\text{m} = 0.2 \text{ min}^{-1}$ ) independently of cues, in line with observations that individual filaments travel approximately their length before reversing (Fig. 2E). Each filament monitors its overlap with filaments in contact with it, where the overlap is defined as the number of neighboring cells on the adjacent filaments a given cell touches, averaged over the filament (“mean cell coordination number”). When a model filament senses a temporal decrease in its

overlap, it reverses its gliding direction after a mean response time  $\tau$ , with smaller values of  $\tau$  representing greater thigmotaxis strength, i.e., a stronger tendency of filaments to stay together. Below, we vary the response time-scale  $\tau$  in the model to determine the effect of thigmotaxis strength on aggregation.

Our model predicts that thigmotactic filaments form organized (highly overlapping) aggregates on a surface (Fig. 3A and movie S11), akin to the dynamic aggregates observed in *T. erythraeum* exposed to menadione (Fig. 2D and movie S10). To quantify aggregation in model simulations, we compute the average overlap over all filaments in the system as a function of time (Fig. 3B). We focus on the three values of thigmotaxis strength, representing filaments that, after detecting a decrease in overlap (which takes  $\sim 10$  s), (i) reverse after a short delay ( $\tau = 0.75$  s, strong thigmotaxis); (ii) reverse after an intermediate delay ( $\tau = 12$  s, medium thigmotaxis); and (iii) reverse after a long delay ( $\tau = 75$  s, weak thigmotaxis). Equivalently, for filaments in a pair moving in opposite directions and risking separation, the three model conditions of strong, intermediate,

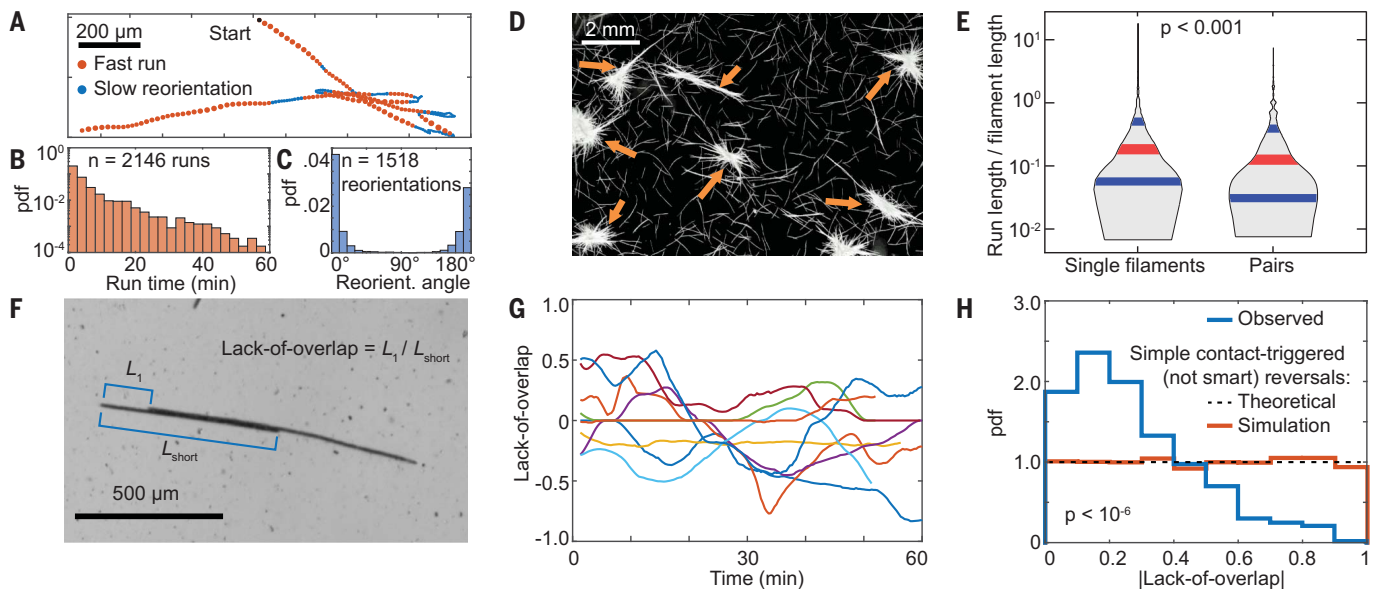


**Fig. 2. Controlled reversals characterize *Trichodesmium* aggregation.**

(A) Trajectory of a filament gliding on a surface, segmented into runs (orange) and reorientations (blue). Dots mark the position of the centroid, with size proportional to instantaneous speed. (B) Run times exhibit a broad distribution. (C) Reorientation angles exhibit a nearly equal repartition between values close to  $0^\circ$  (continuation in the same direction) and values close to  $180^\circ$  (reversals). (D) Midexponential *Trichodesmium* filaments exposed to menadione, which induces oxidative stress, form aggregates (orange arrows). (E) The run length (normalized by filament length) of menadione-exposed *Trichodesmium* is markedly shorter (35% decrease in the mean) for filaments in pairs (two filaments in contact and aligned) than for single filaments [ $n = 12$  independent experiments;  $P < 0.001$ , two-sample one-sided Kolmogorov–Smirnov test ( $n_{\text{single}} = 1964$ ,  $n_{\text{pairs}} = 377$ )]. The gray area shows the distributions as violin

plots. The red line shows the median and the blue lines show the 25th and 75th percentiles. (F) Filament pair illustrating the lack-of-overlap, defined as the fraction of the shorter filament length not overlapping with the longer filament. Lack-of-overlap is positive at one end of the filament pair and negative at the other end. (G) Lack-of-overlap as a function of time for nine filament pairs, illustrating the dynamic rearrangement between filaments. (H) The lack-of-overlap distribution of menadione-exposed filament pairs is strongly skewed toward small lack-of-overlap values compared with the uniform distribution expected if filaments were to simply increase reversal frequency upon contact ( $P < 10^{-6}$ , one-sample two-sided Kolmogorov–Smirnov test,  $n = 53$ ). This is consistent with the hypothesis that *Trichodesmium* performs “smart reversals”, whereby reversals are triggered by an increase in lack-of-overlap as filaments glide upon each other (see text).

and weak thigmotaxis correspond to traveling approximately 4, 15, and 55% of a filament length before performing a smart reversal. For strong thigmotaxis ( $\tau = 0.75$  s), smart reversals lead to the formation of tight aggregates, characterized by high overlap, by preventing filaments from escaping from aggregates (Fig. 3, A and B): when filaments sense a decrease in their overlap with other filaments in the aggregate they rapidly trigger a reversal that on average redirects them toward the aggregate. For strong thigmotaxis, aggregation is robust against filament length variability (fig. S5). Medium ( $\tau = 12$  s) or weak ( $\tau = 75$  s) thigmotaxis strengths result in looser aggregates containing fewer filaments or almost no aggregates, respectively (Fig. 3B). Identifying filament pairs in these simulations shows that the response time  $\tau$  controls the skewness of the lack-of-overlap distribution (Fig. 3C), thus linking the response time  $\tau$ —a core model parameter characterizing smart reversals—with the lack-of-overlap distribution observed in experiments (Fig. 2H). When  $\tau$  is small (strong thigmotaxis), the lack-of-overlap is skewed toward small values (Fig. 3C), in line with our observations (Fig. 2H). As  $\tau$  increases (medium and weak thigmotaxis) the lack-of-overlap distribution becomes more uniform (Fig. 3C).

The response timescale  $\tau$  can be approximately measured in our experiments from the rate of disintegration of filament pairs (Sup-

plementary Text Section VI). These measurements indicate that filaments in menadione correspond to medium-to-strong thigmotaxis in the model, whereas filaments in the control correspond to weak-to-medium thigmotaxis in the model (fig. S5). Additionally, our data show that slower or longer filaments perform stronger thigmotaxis than faster or shorter ones, respectively (Supplementary Text Section VII, table S2).

We also modeled aggregate formation in 3D to show that smart reversals are key to the formation of organized aggregates in a liquid suspension (i.e., away from solid surfaces), such as the marine habitat of *Trichodesmium*. This model represents sequential random arrivals of randomly oriented filaments onto a single seed filament, with which they align upon encounter (Fig. 3D), mimicking, for example, encounters and alignment driven by ocean turbulence (fig. S6, Supplementary Text Sections VIII and IX). We find that strong thigmotaxis converts successive random encounters into an organized aggregate characterized by large overlap (blue curve in Fig. 3D and movie S12). Such large overlap ( $>5$ ), which approaches values characterizing random packing of spheres (41), indicates that a random cell within the aggregate has typically five or more neighboring cells, not including cells on the same filament. Switching off smart reversals after an organized aggregate has

formed (thus leaving only random reversals) leads to rapid disintegration of the aggregate (purple curve in Fig. 3D). Similarly, random reversals alone do not lead to stable aggregates, with filaments only forming small, transient aggregates that continuously disintegrate [for both high ( $2 \text{ min}^{-1}$ ) and low ( $0.4 \text{ min}^{-1}$ ) rates of random reversals, pink and cyan in Fig. 3D]. Additionally, simple adhesion upon encounters, without rearrangement, would result in fractal aggregate morphologies (42) (yellow curve in Fig. 3D and movie S13). Lastly, if filaments stuck to each other and aligned in flow but were otherwise nonmotile they would form elongated chains (red curve in Fig. 3D and movie S14). Both fractals and chains could emerge in scenarios where filaments were nonmotile and sticky. Only strong thigmotaxis produces organized aggregates characterized by large overlap (approximately 5 to 6), whereas all other mechanisms considered above resulted in values of overlap that were at least 50% smaller.

Smart reversals can also explain the rapid, dynamic tightening and loosening of aggregates that we observed upon switches in light intensity (Fig. 1). Modeling the response to an increase and decrease in light intensity as strong and medium thigmotaxis, respectively, reproduces the observed tightening and loosening of aggregates (Fig. 3E). Specifically, the loosening of a compact model aggregate by

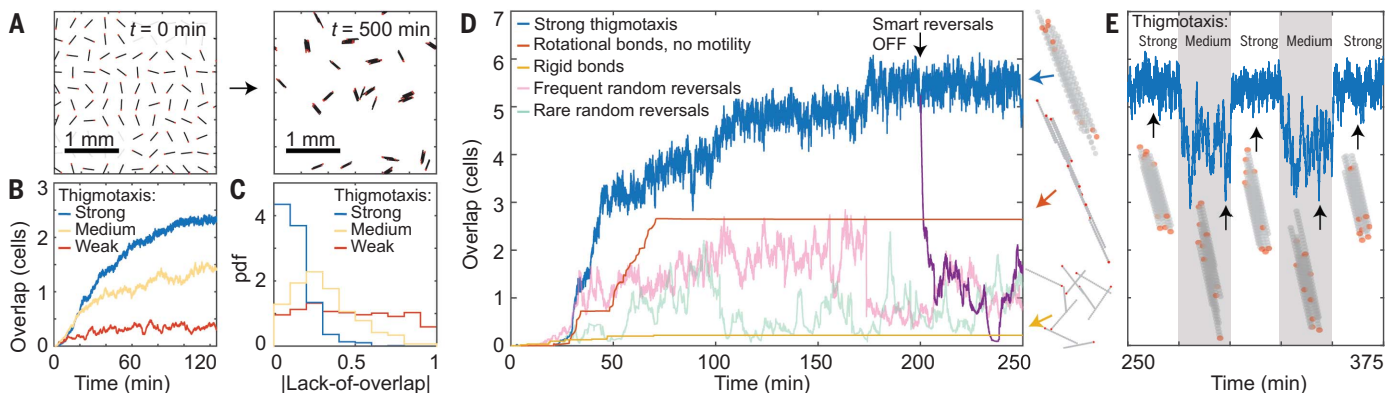


### Fig. 3. Organized aggregate architecture in 3D emerges from smart reversals.

(A) In our 2D model of aggregation on a surface, filaments performing smart reversals ( $\tau = 0.75$  s,  $n = 100$ ), initially separated and oriented randomly on the surface, form aggregates of oscillating filaments (movie S11), akin to those observed experimentally (Fig. 2D). (B) The time course of filament overlap (mean cell coordination number) on a surface for filaments performing smart reversals with different response times ( $\tau = 0.75$  s, blue;  $\tau = 12$  s, yellow;  $\tau = 75$  s, red) shows that tuning the response time directly controls the strength of thigmotaxis: small values of  $\tau$  realize strong thigmotaxis characterized by the emergence of highly overlapping aggregates. Displayed are averages over 6 runs for simulations with 20 filaments. (C) Distribution of the lack-of-overlap of filament pairs identified in 2D simulations (at least  $n = 6$ ) for different thigmotaxis strengths, showing that thigmotaxis skews the lack-of-overlap toward small values, consistent with the experimental observations (Fig. 2H). (D) Overlap as a function of time predicted by 3D simulations of 10 filaments in

suspension. Aggregates form from an initial seed filament that collects other filaments through random encounters. The effect of three possible mechanisms following filament encounter is shown: (i) filaments form rigid bonds and do not rearrange, which creates fractal-like aggregates (yellow); (ii) filaments are not motile and align under external torques (e.g., turbulence-induced), which creates elongated chains (red); or (iii) motile filaments perform smart reversals with strong thigmotaxis ( $\tau = 0.75$  s), which creates compact aggregates (blue). Switching off smart reversals (while retaining random reversals) leads to rapid disintegration of aggregates (purple). Finally, random reversals do not create stable aggregates (pink and cyan). (E) Continuation of the model simulation for the aggregate of filaments executing strong thigmotaxis [blue curve in panel (D)], when the thigmotaxis strength is modulated between strong ( $\tau = 0.75$  s) and medium ( $\tau = 12$  s). The resulting tightening and loosening of the aggregate reproduces the response of aggregates exposed to light switches (Fig. 1).

~30% (measured as the change in overlap in the model; Fig. 3E and movie S15) is akin to the change in aggregate density (a proxy for total overlap) observed experimentally (Fig. 1 and movie S16). Thus, a change in single-filament behavior—modeled as a change in the response time  $\tau$  between detecting a decrease in overlap and reversing—can explain the rapid reshaping of aggregates in response to light switches.

Smart reversals represent an effective mechanism for filaments to remain together after an encounter. These encounters occur differently on a surface versus in the ocean. On a surface, as in most of our experiments, gliding can drive encounters, which occur on the timescale of an hour (fig. S3E). By contrast, in the three-dimensional (3D) water column without surfaces to glide on, encounters are most likely driven by turbulence and buoyancy. The typical encounter timescale between buoyant (density offset  $50 \text{ kg m}^{-3}$ ) individual filaments is <20 hours (43) for a turbulent intensity characteristic of the ocean surface layer ( $10^{-6} \text{ W kg}^{-1}$ ) at an organism concentration representing bloom conditions ( $10^7$  filaments  $\text{m}^{-3}$ ) (44). Consequently, the encounter timescale in the ocean is short enough to convert individual filaments into aggregates within several days, even at tenfold lower concentrations, as we demonstrated using a coagulation model that accounts for aggregate-aggregate encounters (fig. S7, Supplementary Text Section X). By contrast, because *Trichodesmium's* doubling time is a few days (45–47), it would take several weeks for a single filament to grow into a sizeable aggregate, suggesting that encounters are likely faster than growth in driving the formation of aggregates. Still, an encounter timescale of many hours is much longer than the tens of minutes required for a filament to travel its length. Smart reversals protect the nascent aggregate from disintegrating: if filaments lose each other it may be hours before a new filament is encountered. Additionally, turbulence in the ocean surface layer is unlikely to separate a pair of filaments stuck to each other as it exerts shear forces on the order of tens of picoNewtons (Supplementary Text Section X), much smaller than filament adhesive forces, likely mediated by cellular appendages, which are in the range of tens of nanoNewtons (12).

## Discussion

In our experiments, puff-like aggregates are often formed by merging tufts, which in turn could form from disintegrating puffs (movie S4). This sequential formation of puffs is corroborated by dilution experiments, in which only tufts formed (fig. S8). In the ocean, *Trichodesmium* filaments are dilute ( $10^4$  to  $10^6 \text{ m}^{-3}$ ) (3, 6), separated from each other by many filament lengths, corresponding to the conditions of our model of aggregate formation in 3D: puffs may then emerge from encounters between tufts. Puffs may also form

through other mechanisms (e.g., aggregation on dust particles) (14, 48) and some strains may form only puffs or tufts (8, 23). Our work, however, indicates that these two morphologies are less static than currently assumed and can reshape into one another. This might be broadly applicable as most *Trichodesmium* clades (except Clade IV) occur as both tufts and puffs (23). *Trichodesmium* aggregates can constitute different clades (23), corroborating the idea of encounter-driven aggregation. Whether clades can tune smart reversals to avoid other strains such as nondiazotrophic species (49) and thus manipulate aggregate composition remains an open question.

Aggregates have been suggested to form through increased stickiness, mediated by appendages (12) or exopolymers (50). However, our model shows that adhesion alone does not lead to organized aggregates. Although a role for motility in aggregation has been suggested (12, 18, 37), uncoordinated motility would lead to aggregate disintegration and cannot account for reversible aggregate tightening and loosening. Our experiments instead indicate that *T. erythraeum* adjusts its motility in response to a sensory cue, related to the overlap with other filaments. We propose that this response is triggered by surface contact, similar to C-signaling in myxobacteria (51). We find that intrafilament cell-cell autoinduction could plausibly trigger reversals (fig. S9) but more work is needed to unravel molecular mechanisms.

Our work suggests that smart reversals allow *Trichodesmium* to react to environmental changes as transient as shifting cloud cover. Aggregates may loosen to gain exposure to light or tighten to self-shade (in this context, it would be interesting to quantify the response of menadione-treated cultures to changes in light). The transient response we observed suggests that it represents the initial, fastest adaptation to environmental changes ahead of more drastic adaptations (e.g., proteomic reorganization). The rapid changes to aggregate density also modulate exposure to gases and chemicals by the cells and their microbiomes, which may allow them to tune metabolic processes and vertical migration.

*Trichodesmium* aggregation through motility is an example of an active matter system (52, 53). It bears analogies with the formation of fruiting bodies in *Myxococcus xanthus*, resulting from jamming driven by high cell densities, gliding, and reversals (54) and with the behavior of *Pseudomonas aeruginosa*, which avoids jamming by reversing upon contact (55). *Trichodesmium* aggregation is different, however, as its concentration in the ocean is too low for jamming (Supplementary Text Section XI). Instead, *Trichodesmium* uses smart reversals to convert encounters into aggregates. Aggregation also occurs in other filamentous cyanobacteria [e.g., *Oscillatoria terebriformis* (56), *Nostoc punctiforme* (57, 58), and in multispecies fresh-

water cyanospheres (59, 60)]. However, in all cases aggregation mechanisms remain unclear.

Previous work has shown that *Trichodesmium* filaments can wiggle to convey captured iron particles to the core of their aggregate (14, 18, 27). We showed that filament behavior further controls the aggregate's structure itself (fig. S10). Ultimately, the biogeochemical importance of *Trichodesmium*—as a nitrogen fixer, primary producer, and vector of  $\text{CO}_2$  sequestration to depth—hinges on the decentralized yet coordinated behavior of individual filaments.

## REFERENCES AND NOTES

- C. Martínez-Pérez et al., *Nat. Microbiol.* **1**, 16163 (2016).
- E. J. Carpenter, D. G. Capone, in *Nitrogen In The Marine Environment* (Elsevier, 2008), pp. 141–198.
- R. M. Letelier, D. M. Karl, *Mar. Ecol. Prog. Ser.* **133**, 263–273 (1996).
- M. Rodier, R. Le Borgne, *Mar. Pollut. Bull.* **61**, 349–359 (2010).
- I. Bryceson, P. Fay, *Mar. Biol.* **61**, 159–166 (1981).
- E. J. Carpenter, A. Subramaniam, D. G. Capone, *Deep Sea Res. Part I Oceanogr. Res. Pap.* **51**, 173–203 (2004).
- C. S. Davis, D. J. McGillicuddy Jr., *Science* **312**, 1517–1520 (2006).
- A. M. Hynes, E. A. Webb, S. C. Doney, J. B. Waterbury, *J. Phycol.* **48**, 196–210 (2012).
- P. R. F. Bell et al., *Hydrobiologia* **532**, 9–21 (2005).
- L. Prufert-Bebout, H. W. Paerl, C. Lassen, *Appl. Environ. Microbiol.* **59**, 1367–1375 (1993).
- F.-X. Fu, P. R. F. Bell, *Mar. Ecol. Prog. Ser.* **257**, 69–76 (2003).
- Y. Tzubarri, L. Magnezi, A. Be'er, I. Berman-Frank, *ISME J.* **12**, 1682–1693 (2018).
- Y.-B. Chen, J. P. Zehr, M. Mellon, *J. Phycol.* **32**, 916–923 (1996).
- M. Rubin, I. Berman-Frank, Y. Shaked, *Nat. Geosci.* **4**, 529–534 (2011).
- A. E. White, Y. H. Spitz, R. M. Letelier, *Mar. Ecol. Prog. Ser.* **323**, 35–45 (2006).
- K. R. Frischkorn, M. Rouco, B. A. S. Van Mooy, S. T. Dyrhman, *ISME J.* **11**, 2090–2101 (2017).
- K. R. Frischkorn, S. T. Haley, S. T. Dyrhman, *ISME J.* **12**, 997–1007 (2018).
- J. G. Rueter, D. A. Hutchins, R. W. Smith, N. L. Unsworth, in *Marine Pelagic Cyanobacteria: Trichodesmium and other Diazotrophs*, E. J. Carpenter, D. G. Capone, J. G. Rueter, Eds. (Springer, 1992), pp. 289–306.
- K. R. Frischkorn, S. T. Haley, S. T. Dyrhman, *Front. Microbiol.* **10**, 330 (2019).
- M. D. Lee et al., *ISME J.* **11**, 1813–1824 (2017).
- B. A. S. Van Mooy et al., *ISME J.* **6**, 422–429 (2012).
- S. Basu, M. Gledhill, D. de Beer, S. G. Prabh Matondkar, Y. Shaked, *Commun. Biol.* **2**, 284 (2019).
- M. Rouco, S. T. Haley, S. T. Dyrhman, *Environ. Microbiol.* **18**, 5151–5160 (2016).
- M. Eichner, S. Basu, M. Gledhill, D. de Beer, Y. Shaked, *Front. Microbiol.* **10**, 1565 (2019).
- M. J. Eichner et al., *ISME J.* **11**, 1305–1317 (2017).
- M. Eichner et al., *New Phytol.* **222**, 852–863 (2019).
- N. Kessler et al., *ISME J.* **14**, 91–103 (2020).
- N. A. Held et al., *Nat. Microbiol.* **7**, 300–311 (2022).
- T. A. Villareal, E. J. Carpenter, *Microb. Ecol.* **45**, 1–10 (2003).
- M. Benavides et al., *ISME J.* **16**, 2398–2405 (2022).
- M. Rodier, R. Le Borgne, *J. Exp. Mar. Biol. Ecol.* **358**, 20–32 (2008).
- D. G. Capone et al., *Mar. Ecol. Prog. Ser.* **172**, 281–292 (1998).
- D. M. Karl, R. Letelier, D. V. Hebel, D. F. Bird, C. D. Winn, in *Marine Pelagic Cyanobacteria: Trichodesmium and Other Diazotrophs*, E. J. Carpenter, D. G. Capone, J. G. Rueter, Eds. (Springer, 1992), pp. 219–237.
- E. J. Carpenter, D. G. Capone, in *Marine Pelagic Cyanobacteria: Trichodesmium and Other Diazotrophs*, E. J. Carpenter, D. G. Capone, J. G. Rueter, Eds. (Springer, 1992), pp. 211–217.
- K. M. Orcutt et al., *Appl. Environ. Microbiol.* **68**, 2236–2245 (2002).
- N. Blot et al., *Plant Physiol.* **156**, 1934–1954 (2011).
- H. W. Paerl, B. M. Bebout, in *Marine Pelagic Cyanobacteria: Trichodesmium and Other Diazotrophs*, E. J. Carpenter, D. G. Capone, J. G. Rueter, Eds. (1992), pp. 43–59.
- X. Kammerscheit, F. Chauvat, C. Cassier-Chauvat, *Front. Microbiol.* **10**, 1899 (2019).
- S. J. Schnörr, P. J. Steenbergen, M. K. Richardson, D. L. Champagne, *Behav. Brain Res.* **228**, 367–374 (2012).

40. J. Sikora, Z. Baranowski, M. Zajackowska, *Experientia* **48**, 789–792 (1992).
41. L. V. Migal, V. G. Bondarev, N. A. Chekanov, T. P. Bondareva, *J. Phys. Conf. Ser.* **1479**, 012097 (2020).
42. J. R. Rothenbuhler, J.-R. Huang, B. A. DiDonna, A. J. Levine, T. G. Mason, *Soft Matter* **5**, 3639–3645 (2009).
43. J.-A. Arguedas-Leiva, J. Słomka, C. C. Lalescu, R. Stocker, M. Wilczek, *Proc. Natl. Acad. Sci. U.S.A.* **119**, e2203191119 (2022).
44. W. M. Dunstan, J. Hosford, *Bull. Mar. Sci.* **27**, 824–829 (1977).
45. E. Breitbarth, J. Wohlers, J. Kläs, J. LaRoche, I. Peeken, *Mar. Ecol. Prog. Ser.* **359**, 25–36 (2008).
46. C. M. Holl, J. P. Montoya, *J. Phycol.* **44**, 929–937 (2008).
47. M. R. Mulholland, D. G. Capone, *Mar. Ecol. Prog. Ser.* **188**, 33–49 (1999).
48. N. A. Held *et al.*, *ISME Commun.* **1**, 35 (2021).
49. T. O. Delmont, *Proc. Natl. Acad. Sci. U.S.A.* **118**, e2112355118 (2021).
50. I. Berman-Frank, G. Rosenberg, O. Levitan, L. Haramaty, X. Mari, *Environ. Microbiol.* **9**, 1415–1422 (2007).
51. D. Kaiser, *Annu. Rev. Microbiol.* **58**, 75–98 (2004).
52. M. Bär, R. Großmann, S. Heidenreich, F. Peruani, *Annu. Rev. Condens. Matter Phys.* **11**, 441–466 (2020).
53. M. C. Marchetti *et al.*, *Rev. Mod. Phys.* **85**, 1143–1189 (2013).
54. G. Liu *et al.*, *Phys. Rev. Lett.* **122**, 248102 (2019).
55. M. J. Kühn *et al.*, *Proc. Natl. Acad. Sci. U.S.A.* **118**, e2101759118 (2021).
56. R. W. Castenholz, *Nature* **215**, 1285–1286 (1967).
57. A. Wilde, C. W. Mullineaux, *Mol. Microbiol.* **98**, 998–1001 (2015).
58. A. Guljamov *et al.*, *Appl. Environ. Microbiol.* **83**, e01510–e01517 (2017).
59. K. Milferstedt *et al.*, *Sci. Rep.* **7**, 17944 (2017).
60. S. J. N. Duxbury, S. Raguideau, J. Rosko, K. Cremin, M. Coates, C. Quince, O. S. Soyer, Reproducible spatial structure formation and stable community composition in the cyanosphere predicts metabolic interactions. bioRxiv 2022.12.13.520286 [Preprint] (2022); <https://doi.org/10.1101/2022.12.13.520286>.
61. J. Słomka, Data Collection for the article 'Controlled motility in the cyanobacterium *Trichodesmium* regulates aggregate architecture', ETH Research Collection (2022); <https://doi.org/10.3929/ethz-b-000596515>.

#### ACKNOWLEDGMENTS

We thank W. Hess for *Trichodesmium* cultures, E. Borowiecka for help with the figures, and O. Soyer, R. Naisbit, U. Alcolombri, and J. Keegstra for discussions. **Funding:** We gratefully acknowledge funding from an ETH Zurich Postdoctoral Fellowship to U.P.; from an ETH Zurich Postdoctoral Fellowship and a Swiss National Science Foundation Ambizione Grant (PZ00P2\_202188) to J.S.; from an ATTRACT Investigator Grant (A17/MS/11572821/MBRACE) and FNR-CORE Grant (C19/MS/13719464/TOPOFLUME/Sengupta) from the Luxembourg National Research Fund to A.S.; from the Simons Foundation through the Principles of Microbial Ecosystems (PriME) collaboration (grant 542389) to M.A. and (grant 542395) to R.S.; from a Gordon and Betty Moore Foundation Symbiosis in Aquatic Systems Investigator Award (GBMF9197), the Swiss National Science Foundation, National Centre of Competence in

Research (NCCR) Microbiomes (51NF40\_180575), and a Swiss National Science Foundation research grant (205321\_207488) to R.S. **Author contributions:** U.P. and J.S. contributed equally to this work and are listed in alphabetical order. U.P., J.S., A.S., M.A. and R.S. designed research. U.P. and G.S. conducted experiments. J.S. developed mathematical models. U.P., G.S., J.S. and R.S. analyzed data. A.S. provided support with initial experiments and preliminary data analyzes. U.P., J.S., M.A., and R.S. wrote the paper. **Competing interests:** The authors declare no competing interests. **Data and materials availability:** All data are available in the manuscript, the supplementary material or deposited at ETH Research Collection (61). **License information:** Copyright © 2023 the authors, some rights reserved; exclusive licensee American Association for the Advancement of Science. No claim to original US government works. <https://www.sciencemag.org/about/science-licenses-journal-article-reuse>

#### SUPPLEMENTARY MATERIALS

[science.org/doi/10.1126/science.adf2753](https://science.org/doi/10.1126/science.adf2753)

Materials and Methods

Supplementary Text

Figs. S1 to S13

Tables S1 to S3

References (62–77)

MDAR Reproducibility Checklist

Movies S1 to S16

Submitted 11 October 2022; accepted 25 April 2023  
10.1126/science.adf2753



## Controlled motility in the cyanobacterium *Trichodesmium* regulates aggregate architecture

Ulrike Pfreundt, Jonasz Somka, Giulia Schneider, Anupam Sengupta, Francesco Carrara, Vicente Fernandez, Martin Ackermann, and Roman Stocker

*Science*, **380** (6647), .

DOI: 10.1126/science.adf2753

### Editor's summary

The nitrogen-fixing cyanobacterium *Trichodesmium* forms filamentous aggregates in response to stress. Pfreundt *et al.* subjected *Trichodesmium* cultures to excess light and reactive oxygen species, which encouraged them to form aggregates. Analysis of images and videos of individuals and pairs of filaments revealed how their motion affects overall colony architecture. If long segments of filament pairs lose contact with one another, then a change in the direction of their motion ensures that the filaments remain attached. Mathematical modeling demonstrated that responsive filament motion acts as a positive feedback mechanism to maintain aggregate architecture. —Maddy Seale

### View the article online

<https://www.science.org/doi/10.1126/science.adf2753>

### Permissions

<https://www.science.org/help/reprints-and-permissions>

Use of this article is subject to the [Terms of service](#)

---

*Science* (ISSN ) is published by the American Association for the Advancement of Science. 1200 New York Avenue NW, Washington, DC 20005. The title *Science* is a registered trademark of AAAS.

Copyright © 2023 The Authors, some rights reserved; exclusive licensee American Association for the Advancement of Science. No claim to original U.S. Government Works